Effect of surfactant in an airway closure model

F. Romanò, M. Muradoglu, and J. B. Grotberg

Phys. Rev. Fluids **7**, 093103 — Published 21 September 2022

DOI: 10.1103/PhysRevFluids.7.093103

The effect of surfactant in an airway closure model

F. Romanò*

Univ. Lille, CNRS, ONERA, Arts et Métiers Institute of Technology, Centrale Lille, UMR 9014 - LMFL - Laboratoire de Mécanique des Fluides de Lille - Kampé de Fériet, F-59000, Lille, France

M. Muradoglu

Department of Mechanical Engineering, Koc University, Istanbul, Turkey

J. B. Grotberg

Department of Biomedical Engineering, University of Michigan, Ann Arbor, MI, 48109, USA

(Dated: September 6, 2022)

Abstract

A model of the bronchioles lined by the airway surface liquid is employed to investigate the Plateau–Rayleigh instability that can lead to the occlusion of the airways. This physiologically-relevant phenomenon is normally occurring in distal airways, i.e. in the bronchioles from the 7th generation on. Special attention is paid to the effect of surfactant dispersed in the liquid phase and along the liquid-gas interface. A single-layer Newtonian film is simulated in a rigid capillary pipe in order to isolate the impact of the surfactant and unravel their complex dynamics coupled with the multiphase liquid-gas dynamics. Apart from the primary instability leading to airway closure, we focus on the post-coalescence wall stresses and stress gradients produced by the bi-frontal plug growth. With our model, we demonstrate that increasing the surfactant concentration and their strength, the airway closure gets slowed down and the wall stresses are reduced up to 20%. Within the physiological application intended for our model, we study the stability of the multiphase system. We predict the generation at which airway closure will occur depending on the liquid lining thickness and the initial surfactant concentration.

* Email: francesco.romano@ensam.eu

I. INTRODUCTION

Among the several domains one could consider in biological and medical sciences, pulmonology is one the most fruitful in terms of variety of fundamental problems inspiring the fluid mechanics community. At the same time, fundamental studies in respiratory fluid mechanics often provided a guide through the physiological complexity of the problem, highlighting leading-order effects that drive undesired phenomena correlated to widespread pathologies. This is the case, for instance, of the occlusion and reopening of the airways, usually termed *airway closure* and *airway reopening*, respectively, and both explained thanks to classical fluid mechanics arguments.

In fact, the annular liquid coating the bronchioles gives rise to a multiphase flow in a deformable capillary pipe. For the first 15 or 16 airway generations, the multiphase flow involves three phases, i.e. air, mucus and serous or periciliary liquid [1], while the problem becomes a two-phase system (air and a waterish fluid) from the 16th or 17th generation on. In healthy patients, the one- and two-liquid layers lining the inner wall of the airways are relatively thin, ranging from 2% to 4% of the airway radius. However, when pathological conditions lead to hypersecretion of mucus, the relative film thickness can increase up to 40% of the airway radius [2], exceeding the critical threshold after which an infinitesimal perturbation of the air-mucus interface leads to the formation of a liquid plug within a breathing cycle [3]. The resulting *airway closure* can drive the collapse of the corresponding bronchioles [4, 5] and block the air exchange at distal airways. Such a well-documented medical problem has inspired several fluid mechanics models that helped understanding the underlying physical mechanism. The surface tension at the air-mucus interface, responsible of interfacial capillary forces, drives an axial pressure gradient that drains fluid from the thin film coating the airway walls and brings it to the interface bulge until a liquid plug is formed. Such a phenomenon, known as Plateau–Rayleigh instability [6, 7], results from the interfacial pressure jump directly proportional to the surface tension and to the air-mucus interface cross-sectional curvature. These fundamental fluid mechanics problems explain why thicker liquid films are more prone to induce airway closure, as the gas-liquid interface possesses a higher cross-sectional curvature [8]. Moreover, as the instability is driven by surface tension, surfactant replacement therapies are commonly employed to control the Plateau–Rayleigh instability by reducing the average surface tension in order to limit the

occurrence of airway closure events.

Owing to the predictive achievements of theoretical approaches, increasingly refined models have been proposed to study airway closure from first principles. Some of them focused on the onset of the Plateau–Rayleigh instability, relying on a leading-order approximation of the continuity and Navier–Stokes equations valid for thin films. This is the case of [9], who investigated the fluid-elastic instabilities for an airway closure model in deformable capillary pipes, or of [10], who included the effect of surfactant in order to predict how increasing their concentration changes the onset of the capillary instability. Along the same wit, [11] focused on the effect of viscoelasticity on the pre-coalescence phases of distal airway closure. All these studies reliably predict the onset of the instability and, making use of the lubrication theory, they unravelled a number of physiologically interesting effects due to the extension they considered to the canonical Plateau–Rayleigh liquid-lined capillary pipe model, including two-layers lining [12].

As such models rely on the asymptotic thin film approximation, they cannot be used to predict airway closure phases shortly before coalescence and after the liquid plug has been formed. In fact, when the instability-driven interface bulge grows, the thin film asymptotic limit breaks down and more general models must be employed. To investigate such a dynamics, one should rather consider the full Navier–Stokes equation and eventually solve it numerically. This approach has been used by [13], who simulated the whole pre-coalescence process demonstrating that complex three-dimensionalities can arise due to the coupling between the cross-sectional mechanical instabilities of the bronchioles walls and the capillary instabilities of the lining liquid. They showed that the fluid-structure interaction leads to a quicker and fully three-dimensional airway closure. Other models rather focused on the wall stresses and stress gradients produced by a Newtonian airway closure during the pre-coalescence [14] process, showing that they are compatible with a lethal or sub-lethal response of the epithelium [15, 16, 17]. Only recently, the whole closure process has been numerically simulated. By including both, pre- and post-coalescence phases, [8] discovered that the so-called *bi-frontal plug growth* leads to post-coalescence stresses that can be 300% to 600% higher than pre-coalescence values. This is in agreement with corresponding experimental results [18, 19], and it has been confirmed also by [12], who generalized the model to a two-layer coating and found that the airway closure can occur in much shorter times than what predicted by single-layer models. All these studies confirm the potential of air-

way closure in damaging the epithelial cells on the bronchioles wall, and a recent paper of [20] discovered that a viscoelastic instability arising after closure can lead to comparable stress levels for repeated elastic oscillation events triggered by the bi-frontal plug growth for high elastic numbers. Along the same line, corresponding studies have been carried out for the *airway reopening*, investigating the effect of surfactant [21, 22], non-Newtonian effects [23, 24], and compliance of airway walls [25]. For dedicated reviews, we refer the reader to [26, 27, 28, 29].

In this paper we investigate the effect of surfactant on a Newtonian airway closure in an axisymmetric model, including pre- and post-coalescence. Numerical simulations are carried out for biologically-relevant parameters, also relevant to surfactant replacement therapies. The rest of the paper is organized as follows. The problem formulation is presented in Sec. 2. Section 3 deals with the numerical method employed to discretize the mathematical model; Sec. 4 presents the results discussing the effect of the surfactant parameters and the stability properties of the system in light of its physiological interpretation. Finally, Sec. 5 summarizes the paper and draws the conclusions of our study.

II. PROBLEM FORMULATION

We consider an airway closure model aimed at investigating the sole effect of the surfactant in the liquid phase. Within our model framework, fluid-structure interactions and complex rheological properties are neglected, and the two-liquid-layers coating the airway wall is homogenized into a single-layer liquid. To this end, the ciliated epithelium is simplified considering a cylindrical rigid tube of radius a and length L. Airway closure is therefore studied lining the wall with a Newtonian liquid film of dynamic viscosity μ_{L}, density ρ_{L}, and initial average film thickness h. The innermost phase is the gas core of constant dynamic viscosity μ_{G} and density ρ_{G}. The surface tension between the liquid and the gas phase is assumed to depend on the interfacial concentration of surfactant (see fig. 1).

The airway closure is triggered perturbing the interface location by an initial first-Fourier-mode varicose perturbation

$$r = R_{\mathrm{I}}(t=0) = a - h[1 - A \times \cos(2\pi z/L)], \tag{1}$$

where z and r denote the axial and radial coordinates, respectively, t is the time, A is the

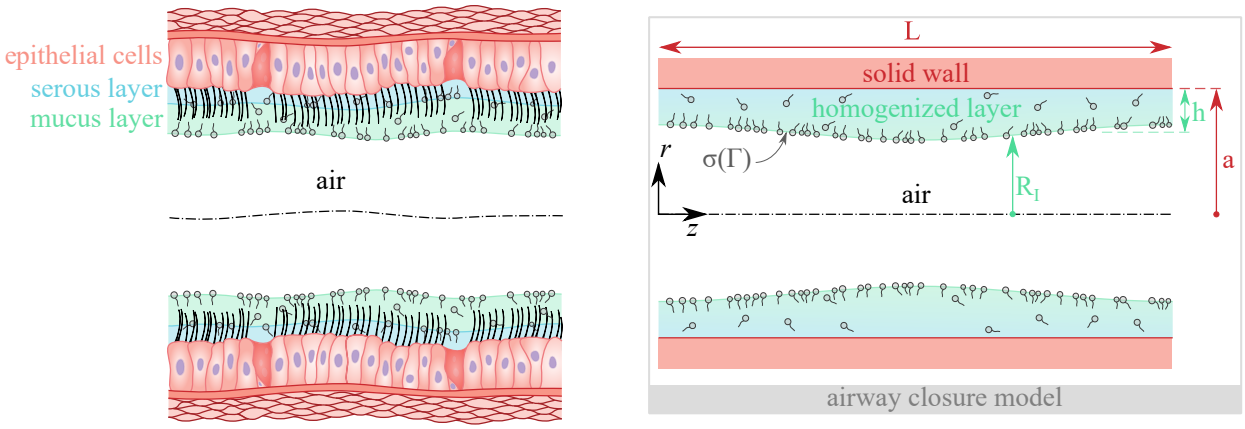

FIG. 1. Schematic of the human airway (left) and the airway model: the ciliated epithelium (left) is simplified to a rigid tube of radius a and length L (light red, right), the coating two-layer non-Newtonian liquid (light blue and light green, left) is modeled by a homogenized layer of average total thickness h (gradient color, right), and the presence of surfactant (gray) is included in both the systems. $R_{\mathrm{I}}(z)$ denotes the radial location of the liquid–gas interface in the airway model.

amplitude of the perturbation and R_{I} is the interface location. Non-dimensionalizing the length, time, pressure and velocity by a, $\mu_{\mathrm{L}}a/\sigma_0$, σ_0/a, $\sigma_0/\mu_{\mathrm{L}}$, respectively, where σ_0 is the reference surface tension (initial average surface tension), the multiphase flow encompassing the gas and liquid phases is governed by the one-field equations [30]

$$\nabla \cdot \vec{u} = 0, \tag{2a}$$

$$\mathrm{La}\left[\frac{\partial\left(\tilde{\varrho}\vec{u}\right)}{\partial t} + \nabla\cdot\left(\tilde{\varrho}\vec{u}\vec{u}\right)\right] = -\nabla p + \nabla\cdot\left[\tilde{\mu}\left(\nabla\vec{u} + \nabla^T\vec{u}\right)\right] + \int_A \left[\sigma(\Gamma)\kappa\vec{n} + \nabla_s\sigma(\Gamma)\right]\delta\left(\vec{x} - \vec{x}_{\mathrm{f}}\right)dA, \tag{2b}$$

where the continuity equation for incompressible flows is defined by (2a), while (2b) is the momentum equation. The spatial and temporal coordinates are denoted by $\vec{x}$ and t, $\vec{u}$ and p are the velocity and pressure fields, respectively, and Γ is the interfacial surfactant concentration normalized with the maximum equilibrium concentration Γ_∞. In the integral, κ is twice the mean curvature, $\vec{n}$ a unit vector normal to the interface, A is the surface area, δ the three-dimensional Dirac delta function, $\vec{x}_{\mathrm{f}}$ denotes the points at the interface, ∇_s is the interface gradient operator along the interface, $\nabla_s = \nabla - \vec{n}\left(\vec{n}\cdot\nabla\right)$, and σ is the surface tension normalized with respect to σ_0 and it is assumed to decrease upon an increase of Γ.

Following [31] and [32], it yields

$$\sigma = \begin{cases} (1 - \beta\Gamma) & \text{if } \Gamma < 1, \\ (1-\beta)\exp\left[\dfrac{\beta(1-\Gamma)}{1-\beta}\right] & \text{if } \Gamma \geq 1. \end{cases} \tag{3}$$

As discussed by [31] and [32], the surface tension σ varies linearly (at leading order) with the interfacial surfactant concentration Γ for $\Gamma < 1$. On the other hand, σ becomes a non linear function of Γ for $\Gamma \geq 1$. In the non-linear regime, the surface tension asymptotically approaches a constant minimum value when the interfacial surfactant concentration reaches the maximum packing value. [31] and [32] assumed an exponential decay of σ for $\Gamma \geq 1$ and thus obtained the present equation of state that well approximates the pulmonary surfactant monolayer. This same equation of state has been also used by other researchers in similar contexts (see e.g. [21, 33]) and it is demonstrated to be a reliable constitutive equation for dilute surfactant concentrations Γ, as the ones considered in this study.

The normal-stress jump due to surface tension and the Marangoni stress at the interface, $\nabla_s\sigma(\Gamma)$, are included by means of the integral, typical of the one-field formulation. Moreover, in the one-field formulation, the physical properties of the multiphase fluid are discontinuously defined over the domain. This is the case of the density and the dynamic viscosity fields, $\tilde{\varrho} = \phi + \varrho(1-\phi)$ and $\tilde{\mu} = \phi + \mu(1-\phi)$, respectively, defined via the indicator function ϕ that equals zero in the gas phase and one in the liquid.

Four non-dimensional groups are identified in (2), which together with the geometric non-dimensional parameters, define the following six dimensionless numbers

$$\mathrm{La} = \frac{\sigma_0\rho_\mathrm{L}a}{\mu_\mathrm{L}^2}, \quad \varrho = \frac{\rho_\mathrm{G}}{\rho_\mathrm{L}}, \quad \mu = \frac{\mu_\mathrm{G}}{\mu_\mathrm{L}}, \quad \beta = \frac{\mathcal{R}T\Gamma_\infty}{\sigma_0}, \quad \lambda = \frac{L}{a}, \quad \varepsilon = \frac{h}{a}, \tag{4}$$

where La is the Laplace number, ϱ and μ are the density and dynamic viscosity ratios, respectively, β is the elasticity number, $\mathcal{R}$ is the ideal gas constant, T is the absolute temperature, λ is the length-to-radius aspect ratio and ε is the average non-dimensional film thickness.

Since the normalized surface tension σ is function of Γ, the following constitutive model for surfactant transport is introduced to complement (2). Scaling the bulk surfactant con-

centration with the critical micelle concentration C_{cmc}

$$\frac{1}{A}\frac{\mathrm{D}(\Gamma A)}{\mathrm{D}t} = \frac{1}{\mathrm{Sc_s La}}\nabla_s^2\Gamma + \dot{S}_\Gamma, \tag{5a}$$

$$\frac{\partial C}{\partial t} + \nabla\cdot(C\vec{u}) = \frac{1}{\mathrm{ScLa}}\nabla\cdot\left(\tilde{D}\nabla C\right) + \dot{S}_C, \tag{5b}$$

where (5a) is the equation derived by [34] to describe the dynamics of interfacial surfactant, and (5b) models the non-dimensional bulk surfactant concentration C by an advection-diffusion equation with a source term, the material derivative is defined as $\mathrm{D}_t = \partial_t + \vec{u}\cdot\nabla$, and the molecular diffusion field for the surfactant in the bulk $\tilde{D} = \phi$ since the molecular diffusion is neglected in the gas phase. The bulk and interfacial surfactant concentration dynamics are coupled by the source terms $\dot{S}_C$ and $\dot{S}_\Gamma$ that describe the transfer of surfactant from the bulk to the surface and vice versa by taking into account the macroscopic adsorption, desorption and saturation phenomena for surfactant at the interface. The $\dot{S}_\Gamma$ is modeled as in [21]

$$\dot{S}_\Gamma = \begin{cases} \dfrac{\mathrm{K_a}}{\mathrm{LaSc_s}}\, C_\mathrm{s}(1-\Gamma) - \dfrac{\mathrm{K_d}}{\mathrm{LaSc_s}}\,\Gamma & \text{if } \Gamma < 1, \\ -\dfrac{\mathrm{K_d}}{\mathrm{LaSc_s}}\,\Gamma & \text{if } \Gamma \geq 1, \end{cases} \tag{6}$$

where C_s is the surfactant concentration in the liquid phase at contact with the interface. The source term in the bulk, $\dot{S}_C$, is dealt with making use of the adsorption layer concept developed by [35], hence by assuming that the transfer of the surfactant mass between the interface and the bulk takes place in a thin layer near the interface. We refer the reader to [35] for more details about the implementation of the bulk and surface source terms, as well as about the detailed interpretation of the adsorption layer.

Five new non-dimensional groups arise due to (5)

$$\mathrm{Sc} = \frac{\mu_\mathrm{L}}{\rho_\mathrm{L} D_\mathrm{L}}, \quad \mathrm{Sc_s} = \frac{\mu_\mathrm{L}}{\rho_\mathrm{L} D_\mathrm{S}}, \quad \mathrm{K_a} = \frac{k_\mathrm{a} C_{\mathrm{cmc}} a^2}{D_\mathrm{S}}, \quad \mathrm{K_d} = \frac{k_\mathrm{a} a^2}{D_\mathrm{S}}, \quad \chi = \frac{\Gamma_\infty}{C_{\mathrm{cmc}} a}, \tag{7}$$

where Sc is the bulk Schmidt number, $\mathrm{Sc_s}$ the interfacial Schmidt number, $\mathrm{K_a}$ and $\mathrm{K_d}$ are the non-dimensional adsorption and desorption coefficients, χ is the penetration depth (derived from the redistribution of surfactant mass in the adsorption layer), D_S and D_L are the molecular diffusion coefficients on the interface and in the bulk (in liquid phase), respectively, and k_a and k_d are the adsorption and the desorption coefficients. Finally, we

also assume that the material properties remain constant following the fluid trajectory

$$\frac{\mathrm{D}\tilde{\varrho}}{\mathrm{D}t} = 0, \qquad \frac{\mathrm{D}\tilde{\mu}}{\mathrm{D}t} = 0, \qquad \frac{\mathrm{D}\tilde{D}}{\mathrm{D}t} = 0. \tag{8}$$

III. NUMERICAL METHOD

The Finite-Difference/Front-Tracking (FD/FT) method of [35, 36] is used to discretize the continuity and Navier–Stokes equations (2) fully coupled with the evolution model for the bulk and interfacial surfactant concentration (5). The projection method of [37, 38] is applied to a staggered Eulerian grid for discretizing the bulk equations, i.e. (2) and (5b), and preserving the coupling between them. The numerical scheme is second-order accurate in space for all the terms of the system except for the convective term of the advection-diffusion equation (5b), for which we use the fifth-order WENO-Z scheme of [39]. Owing to the small time step requirements for preserving the numerical stability of the discrete problem, the time derivatives are discretized by a first-order accurate scheme. This approach is found to minimize the computational cost, keeping the share of the temporal error negligible with respect to the spatial one.

In combination with the steady Eulerian grid, a Lagrangian grid consisting of marker points and in-between front elements is simply advected in the domain by the local flow velocity computed on the Eulerian grid. The marker points and the front elements of the Lagrangian grid are used to track the liquid–gas interface and to solve the interfacial surfactant concentration equation (5a). The same spatial and temporal accuracy is used for (5a) as for the bulk equations discretized on the Eulerian grid. Unlike the Eulerian grid, the Lagrangian grid is reconstructed at every time step either adding or removing front elements and markers. This is necessary to prevent a too dense or a too coarse discrete front, and to deal with topological changes of the interface. The reader is referred to [30] for detailed information about the Lagrangian grid reconstruction, and to [21, 40] for a sensitivity analysis on the numerical parameters used when topological changes of Lagrangian grid are implemented in our front-tracking method for airway reopening problems. Special attention is paid to maintain strict mass conservation of the interfacial surfactant concentration Γ when reconstructing the Lagrangian grid. For more details about the mass-conservative algorithm in use in this study, we refer to [35].

The synergistic use of Eulerian and Lagrangian approaches is not only limited to the advection of the front. In fact, after tracking the interface, the indicator function ϕ is reconstructed on the Eulerian grid at each time step based on the location of the Lagrangian front (see [41]). Such indicator function is used to set the fluid properties $\tilde{\varrho}$, $\tilde{\mu}$ and $\tilde{D}$, to compute the bulk surfactant concentration in the immediate proximity of the liquid–gas interface C_{s}, and to distribute the source term $\dot{S}_C$ following the adsorption layer model of [35]. Finally, the computation of the surface tension is carried out on the Lagrangian grid and then transferred to the Eulerian staggered grid points by means of Peskin's cosine distribution functions [42], which are included in (2b) by using a body-force approach [41].

The FD/FT code used in this study has been extensively tested for airway closure and airway reopening problems including surfactant and topological changes of the interface. The most recent comparisons of our code with other numerical solvers and experimental results are reported in [8, 20, 21] for parameters relevant to our investigation. Such studies demonstrate the satisfactory accuracy of our FD/FT code, hence we refer the reader to them rather than further validating our solver.

IV. RESULTS AND DISCUSSION

The liquid plug formation in adult human lungs is the investigation framework of our study, with a special focus on the effect of surfactant throughout the whole process. Since we are interested in surface-tension dominated flows, where airway closure is physiologically relevant, we limit our study to small bronchioles for which gravitational effects can safely be neglected (as assumed by (2b)). Hence, to characterize a regime for which gravitational forces are negligible, we consider the static Bond number Bo

$$\mathrm{Bo} = \frac{g a^2 (\rho_{\mathrm{L}} - \rho_{\mathrm{G}})}{\sigma_0} \tag{9}$$

where g is the gravitational acceleration.

For the first 14 lung generations the power-law fit of [43] holds, i.e. $a_n = a_0 2^{-n/3}$, where $a_0 \in [0.75,\ 1]$ cm is the radius at the 0-th generation (trachea) and a_n is the radius at the n-th generation (see e.g. [44]). Considering that, for healthy conditions, the mucus-to-air mean surface tension is $\sigma_0 \approx 20$dyn cm^{-1}, and for pathological conditions $\sigma_0 \approx 50$dyn cm^{-1} [45], and assuming $\rho_{\mathrm{L}} \approx 1$ g cm^{-3} and $\rho_{\mathrm{G}} \approx 10^{-3}$ g cm^{-3}, the static bond number

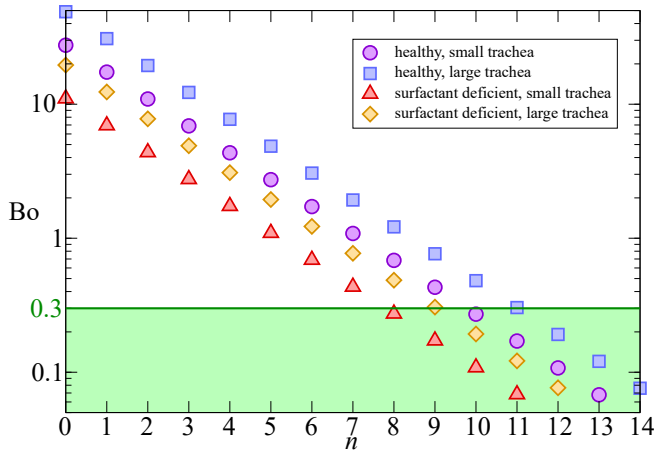

FIG. 2. Order-of-magnitude estimate of the static Bond number as function of the lung generation. The green area denotes the working framework of our investigation for which gravitational effects are safely neglected (Bo < 0.3).

as function of the lung generations is depicted in fig. 2. Based on this order-of-magnitude estimate, for individuals with surfactant deficiency and a small trachea (i.e. $a_0 = 0.75$ cm and $\sigma_0 \approx 50$dyn cm^{-1}), the gravitational effects can be neglected already starting from generation 8. On the other hand, for healthy patients with a large trachea (i.e. $a_0 = 1$ cm and $\sigma_0 \approx 20$dyn cm^{-1}), gravitational effects are negligible only from the 11th generation on. Healthy patients with small trachea and pathological cases with large trachea lie in between, i.e. 10th and 9th generation, respectively.

Based on this characterization of the small-Bond-number regime (Bo < 0.3), we conclude that the range of the mucus-to-air Laplace number of interest for our model should consider airways from the 8th generation on for small tracheas (i.e. $a < 0.12$ cm) if the patient suffers of surfactant deficiency ($\sigma_0 \approx 50$dyn cm^{-1}) and from the 10th generation on for small tracheas (i.e. $a < 0.07$ cm) if the patient is healthy ($\sigma_0 \approx 20$dyn cm^{-1}). This latter case leads to higher Laplace numbers. Considering that the dynamic viscosity of mucus may vary over several orders of magnitudes, ranging from 10 to 10000 times larger than that of water, i.e. $\mu_M \in [0.1,\ 100]$ poise, the Laplace number is La $\lesssim 350$. We will then consider a baseline case with La $= 100$ and slightly enlarge the range of admissible Laplace numbers to make sure that all the physiologically-relevant La are taken into account, i.e. La $= [50,\ 500]$. Following [8, 20], the length-to-radius ratio of the airway is set equal to $\lambda = 6$, while the

non-dimensional film thickness is considered to vary within the range $\varepsilon \in [0.125,\ 0.3]$, which includes biologically-relevant values. These values of normalized thickness for the *airway surface liquid* (terminus technicus in the corresponding physiology literature) exceed the ε for regular healthy conditions ($\varepsilon \approx 0.05$). The range of ε selected in our study rather applies to the airway mucus accumulation extensively reported by physiologists as a result of the conversion of water-secreting serous cells into mucus secreting cells induced by asthma, chronic bronchitis, cystic fibrosis and other inflammatory lung diseases [46]. Moreover, we set $A = 10\%$ as in [8, 20]. The choice of this amplitude is made considering that the mechanism at the core of the airway closure is the Plateau–Rayleigh instability, which is a linear instability. This means that the interface perturbation grows exponentially until it is small enough. Hence, only large-enough initial perturbations are of physiological relevance as they lead to airway closures that develop in a time shorter than a typical breathing cycle. The expected critical mode is $2\pi \approx \lambda = 6$, hence the most dangerous mode (1) is still dominant over the others. We stress, however, that nonlinear effects due to non-modal initial conditions could impact the capillary drainage of coating films and collars (see [47]), but they are out of the scope of this study.

For pulmonary surfactant, the critical micelle bulk concentration is $C_{\mathrm{cmc}} \approx 10^{-3}$ g/cm^3 and the adsorption and desorption kinetics are $k_a \approx 1.7{\times}10^3$ cm^3/g·s and $k_d \approx 1.7{\times}10^{-2}$ 1/s [48, 49]. According to the measurements of [50], the surface diffusivity of pulmonary surfactant is $D_s \in [10^{-7}, 7\times10^{-7}]$ cm^2/s, which leads to baseline values of the non-dimensional absorption and desorption coefficients of $\mathrm{K_a} = 10^4$ and $\mathrm{K_d} = 10^2$, respectively. In our study, we will carry out a sensitivity analysis for these two parameters within the ranges $\mathrm{K_a} \in [10^3,\ 10^5]$ and $\mathrm{K_d} \in [10,\ 10^3]$, as done in [21]. Following the estimate of [51], the maximum equilibrium interfacial concentration for pulmonary surfactant is $\Gamma_\infty \approx 3.1\times10^{-7}$ g/cm^2, hence the baseline value of the dimensionless adsorption depth is assumed to be $\chi \approx 0.01$. The importance of χ will however be tested within the range $\chi \in [0.001,\ 1]$. Finally, following [31], the baseline Schmidt numbers are set to $\mathrm{Sc_s} = 100$ and $\mathrm{Sc} = 10$ and following [48], the baseline value of the elasticity number is set to $\beta = 0.7$. A sensitivity analysis to such parameters choice will be carried out considering the ranges $\mathrm{Sc_s} \in [10,\ 100]$ and $Sc \in [1,\ 10]$, as done in [21].

A. Analysis of surfactant effects in a typical airway closure scenario

A typical airway closure scenario is here presented by simulating our model for the baseline parameters, i.e. La = 100, $C_0 = 10^{-4}$, $\beta = 0.7$, Sc = 10, $\mathrm{Sc_s} = 100$, $\mathrm{K_a} = 10^4$, $\mathrm{K_d} = 10^2$, $\chi = 0.01$, and $\varepsilon = 0.25$. Figure 3 depicts the dynamics of the liquid-lined system initially perturbed by a varicose perturbation of 10% of amplitude. The Plateau–Rayleigh instability develops naturally in such a configuration, draining liquid from the thin film at the wall and driving it towards the bulge where the pressure has its minimum (see bottom panel at $t = 525$ in fig. 3). This is due to the surface tension at the liquid-gas interface that reduces the pressure proportionally to the local cross section curvature of the interface (R_{I}^{-1}). The more the fluid gets drained from the thin film and transported to the bulge, the more the pressure at the bulge decreases with respect to the thin-film pressure, the faster the draining, the faster the bulge grows. On the other hand, for thinner liquid film at the wall it becomes increasingly difficult to drain liquid. As a result, if the initial liquid lining the airway wall is thick enough, the surface tension destabilization overcomes the increasing draining resistance of the thin film and the Plateau–Rayleigh instability leads to the formation of a liquid plug (occurring between $t = 885$ and $t = 900$ in fig. 3), and to a successive *bi-frontal plug growth* responsible of a significant increase of stresses at the airway wall [8]. It is expected therefore that an increase of the surface tension (hence of the Laplace number La) will further destabilize the interface driving a quicker airway closure. On the other hand, a thinner initial film thickness (ε) would rather tend to oppose the closure of the airway, slowing it down or even preventing it by leading to the thin film pinch-off.

Such a well understood dynamics has been extensively reported in literature and it holds for Newtonian single- and double-layer coating, as well as for viscoelastic airway closure [8, 12, 14, 18, 20]. In this paper, we aim at investigating the effects of surfactant that locally reduce the surface tension and create Marangoni stresses, i.e. interfacial stresses that drive the flow along the interface from low to high surface tension regions. The top panels in fig. 3 report the scalar field of surfactant concentration in the bulk C normalized with C_0, $\tilde{C}$, together with the interfacial surfactant concentration Γ depicted in red. In the initial phases of the liquid plug formation, the Γ remains almost uniformly distributed along the interface, leading to an effective reduction of the average surface tension σ_0, hence of the average Laplace number (average of the local Laplace number based on the local surface

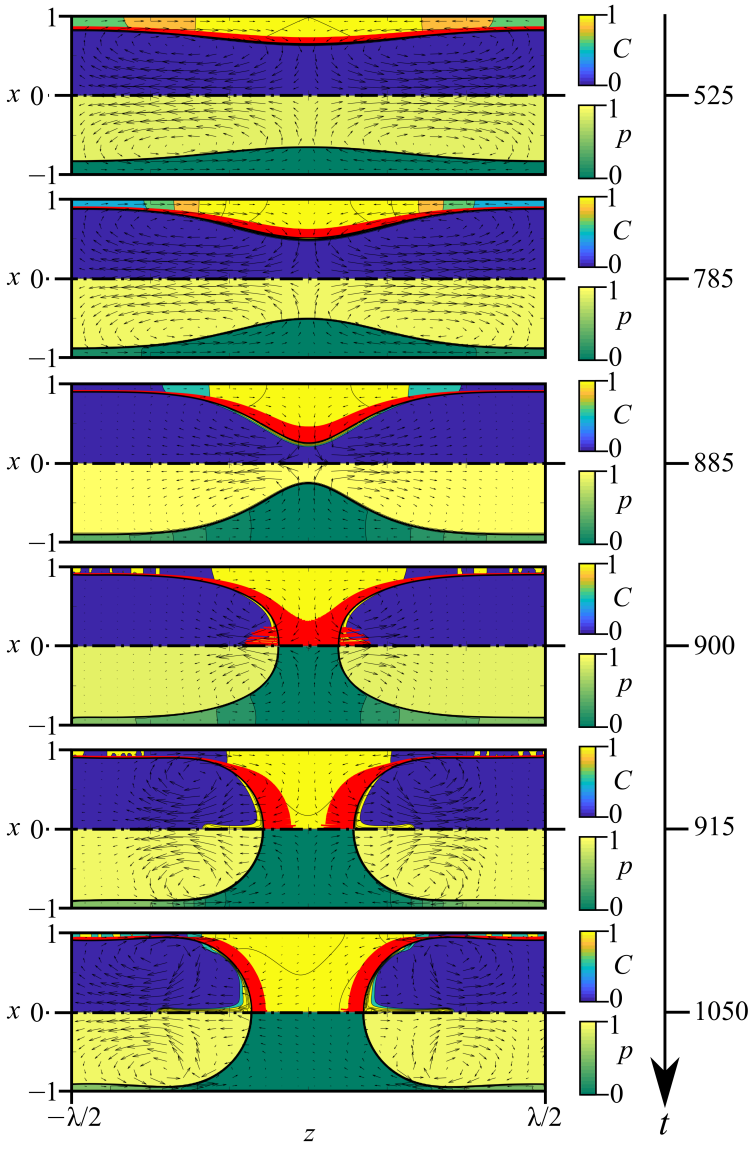

FIG. 3. Airway closure for La = 100, $C_0 = 10^{-4}$, $\beta = 0.7$, Sc = 10, $\mathrm{Sc_s} = 100$, $\mathrm{K_a} = 10^4$, $\mathrm{K_d} = 10^2$, $\chi = 0.01$, and $\varepsilon = 0.25$. Top panels: Surfactant concentration in the bulk C normalized with C_0, $\tilde{C}$. The surfactant concentration at the interface Γ is depicted by red segments normal to the interface whose length is proportional to Γ. Bottom panels: pressure field. The arrows denote the flow velocity and the thick black line depicts the interface.

tension). Marangoni stresses are of minor importance during the early pre-coalescence phase (see $t = 525$ in fig. 3). The draining of liquid from the thin film to the bulge tends, however, to transport the surfactant towards the center of the capillary pipe leading to an increase of the surface tension gradient, hence of the Marangoni stress. As the surface tension at

the bulge is lower than that at the thin film, the corresponding solutocapillary effect tends to oppose the airway closure pulling the interface from low-surface-tension (bulge) towards high-surface-tension regions (thin film). The combined effect of the surfactant distributed on the interface is therefore a twofold net stabilizing effect for the Plateau–Rayleigh instability: (i) the reduction of the average Laplace number limits the impact of the capillary instability, and (ii) the Marangoni stresses along the interface tend to redistribute the liquid from the bulge towards the thin film. It is therefore expected that increasing the initial concentration of surfactant will slow down the airway closure (see the following sections for a quantitative analysis).

The post-coalescence phase is interpreted along the same line. In fact, the strong interfacial concentration of surfactant initially distributed at the interface of the two retracting air fingers leads to two simultaneous effects. On the one hand, the local reduction of surface tension slows down the recovery of a spherical-cap shape of the interface. On the other hand, the Marangoni stress drives fluid from the liquid plug to the thin film, playing in favour of an ellipsoidal interfacial geometry (see $t = 900$ and $t = 915$ in fig. 3). The further draining leading to the bi-frontal plug growth tends however to recover the equilibrium condition for the interface, leading to a quasi-spherical shape for the trailing fronts of the two retracting air fingers in the airway closure model.

Such a non-trivial dynamics will be further investigated in the following sections, with a special focus on the stress and stress gradients at the airway wall, owing to their physiological significance for the bronchioles epithelium.

B. Effect of the initial bulk surfactant concentration C_0 and elasticity number β

The effect of bulk surfactant concentration is investigated carrying out a parametric study on the initial bulk concentration $C_0 \in [10^{-5},\ 5 \times 10^{-4}]$, and keeping all the other model parameters fixed, i.e. for $\mathrm{La} = 100$, $\beta = 0.7$, $\mathrm{Sc} = 10$, $\mathrm{Sc_s} = 100$, $\mathrm{K_a} = 10^4$, $\mathrm{K_d} = 10^2$, $\chi = 0.01$, and $\varepsilon = 0.25$. The relevance of this parametric study is motivated either by pathological conditions corresponding to a surfactant deficiency, or by surfactant replacement therapies commonly in use as medical treatments to favour airway reopening and inhibit successive liquid plug formation.

Upon an increase of the bulk surfactant concentration C_0, the average surface tension

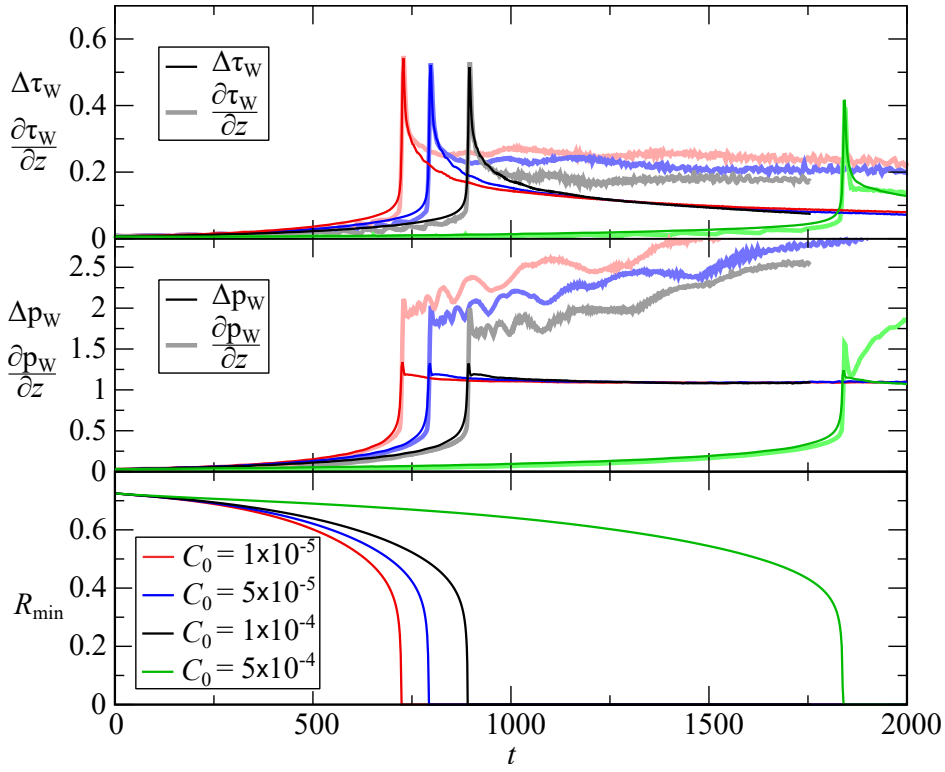

FIG. 4. Effect of the bulk surfactant concentration. Bottom: minimum of the radial location of the interface, R_I (solid line). Middle: excursion of the normal stress distribution along the wall, $\Delta p_{\mathrm{w}}(t) = \max_z p(r=1) - \min_z p(r=1)$ (light-colored bold line), and the maximum axial wall pressure gradient $\max|\partial_z p(r=1)|$ (dark-colored line). Top: excursion of the tangential stress distribution along the wall, $\Delta\tau_{\mathrm{w}}(t) = \max_z \tau(r=1) - \min_z \tau(r=1)$ (light-colored bold line), and the maximum axial wall shear stress gradient $\max|\partial_z \tau(r=1)|$ (dark-colored line). The bulk surfactant concentration C_0 is varied between 10^{-5} and 5×10^{-4}, whereas the other simulation parameters are fixed: $\mathrm{La}=100$, $\beta=0.7$, $\mathrm{Sc}=10$, $\mathrm{Sc_s}=100$, $\mathrm{K_a}=10^4$, $\mathrm{K_d}=10^2$, $\chi=0.01$, and $\varepsilon=0.25$.

decays non-uniformly all along the liquid-gas interface and leads to a net decrease of the average local Laplace number $\overline{\mathrm{La}} = \langle \mathrm{La}\sigma/\sigma_0 \rangle < \mathrm{La}$, as well as to a redistribution of Marangoni stresses induced by the surface tension gradients. For the considered parameters, the reduction of average capillary stresses dominates over the impact of Marangoni stresses, that are (of minor) relevance only for the liquid plug dynamics immediately prior and post closure. As a result, fig. 4 demonstrates that increasing C_0 slows down the Plateau–Rayleigh instability leading to a longer closure time t_{c}. We remark, however, that the relative increment

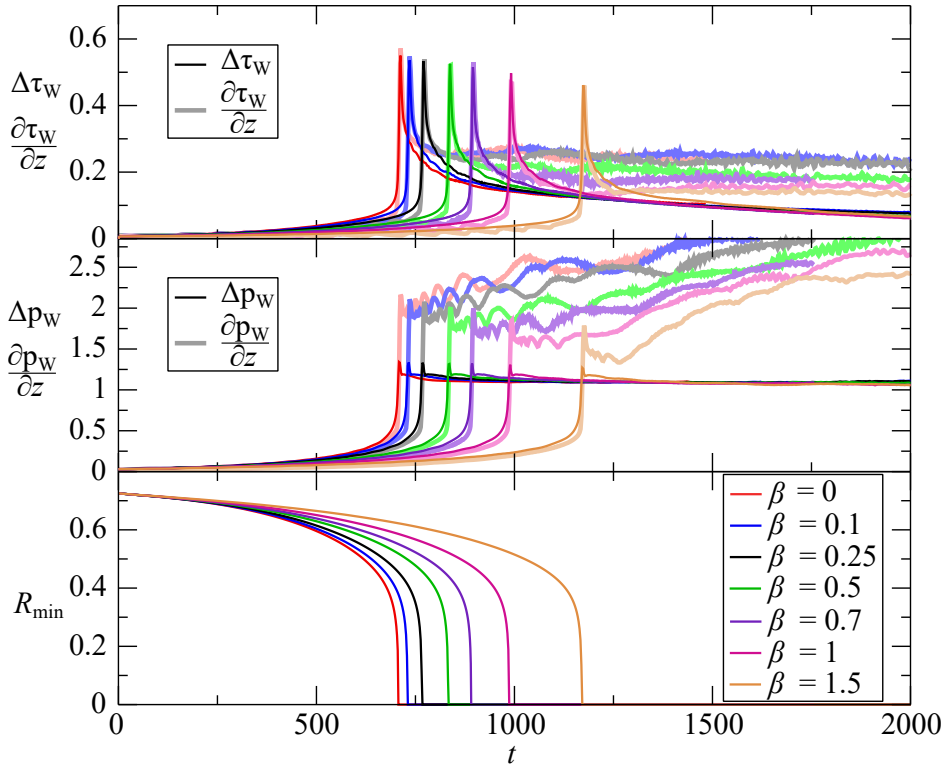

FIG. 5. Effect of the elasticity number, i.e. the strength of the surfactant. Bottom: minimum of the radial location of the interface, R_I (solid line). Middle: excursion of the normal stress distribution along the wall, $\Delta p_{\rm w}(t) = \max_z p(r=1) - \min_z p(r=1)$ (light-colored bold line), and the maximum axial wall pressure gradient $\max|\partial_z p(r=1)|$ (dark-colored line). Top: excursion of the tangential stress distribution along the wall, $\Delta\tau_{\rm w}(t) = \max_z \tau(r=1) - \min_z \tau(r=1)$ (light-colored bold line), and the maximum axial wall shear stress gradient $\max|\partial_z \tau(r=1)|$ (dark-colored line). The elasticity number β is varied between 0 and 1.5, whereas the other simulation parameters are fixed: $C_0 = 10^{-4}$, La $= 100$, Sc $= 10$, Sc$_{\rm s} = 100$, K$_{\rm a} = 10^4$, K$_{\rm d} = 10^2$, $\chi = 0.01$, and $\varepsilon = 0.25$.

of the closure time is strongly non-linear. In fact, for small bulk surfactant concentrations, by multiplying C_0 of a factor 5, i.e. increasing from $C_0 = 10^{-5}$ to $C_0 = 5 \times 10^{-5}$, leads to a relative increment of $t_{\rm c}$ of about 10%. On the other hand, for the highest surfactant concentrations considered, increasing by a factor 5 C_0, i.e. increasing from $C_0 = 10^{-4}$ to $C_0 = 5 \times 10^{-4}$, almost doubles the closure time producing a relative increment of $t_{\rm c}$ of about 100%. This can be understood considering the non-linear decrease of surface tension upon an increase of the interfacial surfactant concentration Γ for $\Gamma \geq 1$ (see (3)).

The impact of the bulk surfactant concentration on the wall stresses is however less

significant. Monitoring the tangential wall stress excursions, $\Delta\tau_{\mathrm{w}}(t) = \max_z \tau(r=1) - \min_z \tau(r=1)$, fig. 4 shows only minor changes of the stress peaks for $C_0 \leq 10^{-4}$, and increasing the bulk surfactant concentration to $C_0 = 5\times10^{-4}$ decreases the tangential stress peak of about 20% with respect to $C_0 = 10^{-4}$. The quantitative characterizations of such a non-linear process is affected by the model, hence they are accurate if a linear decrease of σ with Γ is dominant for $\Gamma < 1$ and it asymptotically transitions to the Langmuir adsorption model [52] for $\Gamma > 1$. Quantitatively consistent observations are done for the maximum tangential stress gradients $\max|\partial_z\tau_{\mathrm{w}}|$, while the peak normal wall stress excursions, $\Delta p_{\mathrm{w}} = \max_z p(r=1) - \min_z p(r=1)$, are essentially not affected by C_0 even for the highest bulk surfactant concentrations considered. A more remarkable impact is demonstrated in fig. 4 for the maximum axial wall pressure gradient $\max|\partial_z p(r=1)|$. This is in agreement with the observations of [8], who correlated the peak of $\max|\partial_z p_{\mathrm{w}}|$ to the capillary wave originated near the wall right after the *bi-frontal plug growth* that enlarges the liquid plug. The net decrease of the local Laplace number due to the increase of surfactant concentration leads to weaker capillary stresses, hence to weaker $\max|\partial_z p_{\mathrm{w}}|$.

The same qualitative impact on the airway closure process observed upon an increase of the initial bulk concentration C_0, is also reproduced by an increase of the elasticity number β. This is demonstrated in fig. 5 by varying $\beta \in [0,\ 1.5]$ and fixing all the other model parameters to the baseline values, i.e. $C_0 = 10^{-4}$, $\mathrm{La} = 100$, $\mathrm{Sc} = 10$, $\mathrm{Sc_s} = 100$, $\mathrm{K_a} = 10^4$, $\mathrm{K_d} = 10^2$, $\chi = 0.01$, and $\varepsilon = 0.25$. In fact, increasing β enhances the impact of the interfacial surfactant concentration Γ on the surface tension (see (3)). This leads to a reduction of the effective Laplace number that slows down the Plateau–Rayleigh instability and reduces the shear stress $\Delta\tau_{\mathrm{w}}$ and shear stress gradient $\max|\partial_z\tau_{\mathrm{w}}|$ at the wall. Moreover, increasing β is also impactful on the capillary wave propagating due to the bifrontal plug growth. As a result, the pressure gradient at the wall is tamed down by strong surfactants (high β).

Beside the reduction of the effective Laplace number, an increase of β induces a variation of the Marangoni stresses. For $\beta = 0$, the surface tension is constant and the interfacial surfactant distribution does not induce any extra driving to the system. In this case, the surfactant plays the role of a passive tracer that can be absorbed and desorbed at the liquid-gas interface, but its concentration does not affect the liquid plug dynamics. For $\beta \neq 0$, the surfactant dynamics gets two-way coupled to the momentum equation via the interfacial gradient of surface tension. This leads to a rapid increase of the Marangoni stresses, well

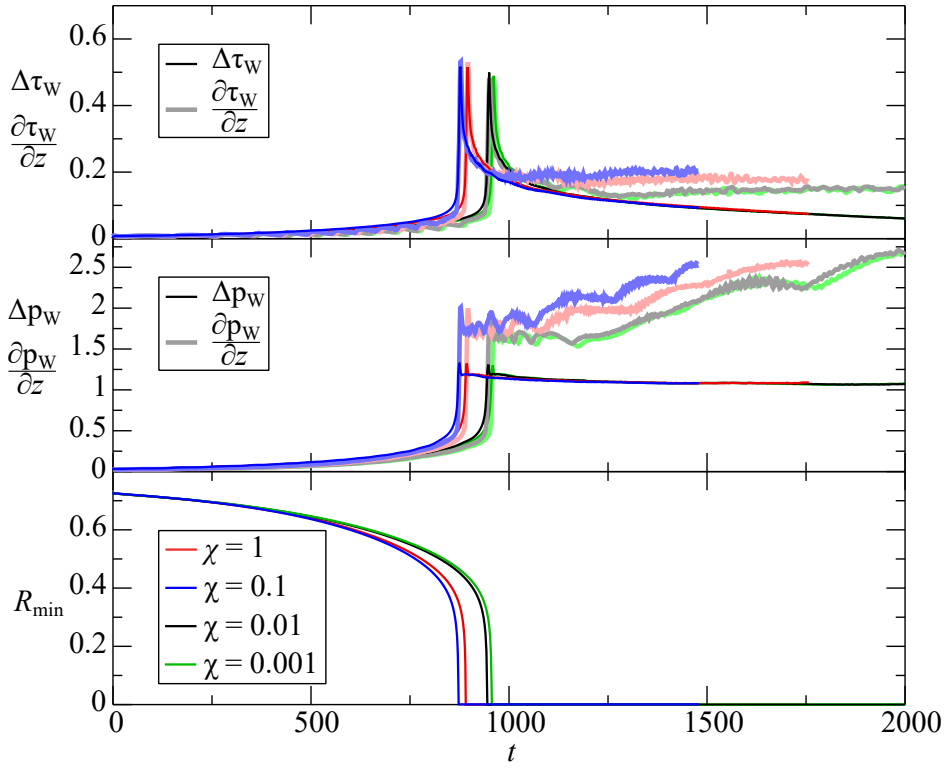

FIG. 6. Effect of the adsorption depth. Bottom: minimum of the radial location of the interface, R_I (solid line). Middle: excursion of the normal stress distribution along the wall, $\Delta p_{\rm w}(t) = \max_z p(r=1) - \min_z p(r=1)$ (light-colored bold line), and the maximum axial wall pressure gradient $\max|\partial_z p(r=1)|$ (dark-colored line). Top: excursion of the tangential stress distribution along the wall, $\Delta\tau_{\rm w}(t) = \max_z \tau(r=1) - \min_z \tau(r=1)$ (light-colored bold line), and the maximum axial wall shear stress gradient $\max|\partial_z \tau(r=1)|$ (dark-colored line). The penetration depth χ is varied between 0.001 and 1, whereas the other simulation parameters are fixed: $C_0 = 10^{-4}$, La $= 100$, Sc $= 10$, Sc$_{\rm s} = 100$, K$_{\rm a} = 10^4$, K$_{\rm d} = 10^2$, $\beta = 0.7$, and $\varepsilon = 0.25$.

quantified by the Marangoni number Ma $= -\partial_\Gamma \sigma R C_0/\mu_{\rm L} D_{\rm L}$. Such an increase saturates when the driving becomes too strong and concentrates the surfactant in a small portion of the interface, making $-\partial_\Gamma\sigma$ pass from $-\partial_\Gamma\sigma = \beta$ for $\Gamma < 1$ to $-\partial_\Gamma\sigma(\beta) = \beta\exp(\beta(1-\Gamma)/(1-\beta))$ for $\Gamma \geq 1$. As observed by increasing C_0, the Marangoni driving represents an higher-order correction when compared to the reduction of the effective Laplace number.

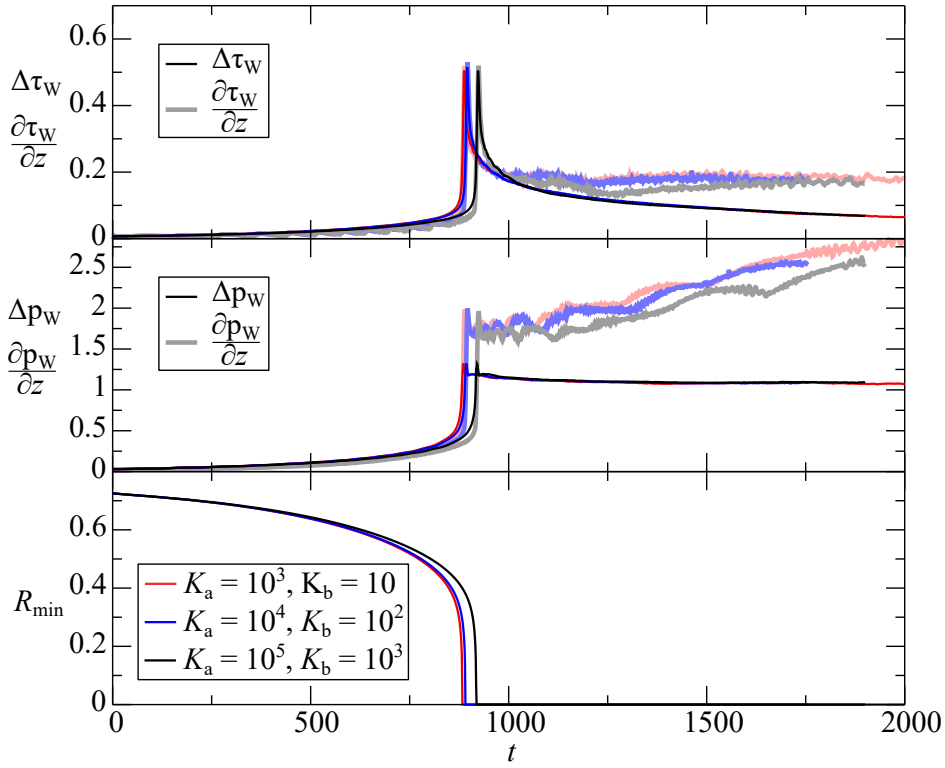

FIG. 7. Effect of the adsorption and desorption coefficients. Bottom: minimum of the radial location of the interface, R_I (solid line). Middle: excursion of the normal stress distribution along the wall, $\Delta p_w(t) = \max_z p(r=1) - \min_z p(r=1)$ (light-colored bold line), and the maximum axial wall pressure gradient $\max|\partial_z p(r=1)|$ (dark-colored line). Top: excursion of the tangential stress distribution along the wall, $\Delta\tau_w(t) = \max_z \tau(r=1) - \min_z \tau(r=1)$ (light-colored bold line), and the maximum axial wall shear stress gradient $\max|\partial_z \tau(r=1)|$ (dark-colored line). The adsorption and desorption coefficients, i.e. K_a and K_d, respectively, are varied between $(K_a,\ K_d) \in ([10^3,\ 10^5],\ [10,\ 10^3])$, whereas the other simulation parameters are fixed: $C_0 = 10^{-4}$, La $= 100$, Sc $= 10$, $Sc_s = 100$, $\chi = 0.01$, $\beta = 0.7$, and $\varepsilon = 0.25$.

C. Effect of the adsorption K_a and desorption K_d coefficients, penetration depth χ, and Schmidt numbers Sc and Sc_s

Except for β that directly act on σ, all the other non-dimensional groups characterizing the physicochemical properties of the surfactant exert their impact on the liquid plug by affecting Γ. This is the case of the adsorption K_a and desorption K_d coefficients, of the penetration depth χ, and of the Schmidt numbers Sc and Sc_s.

Figure 6 demonstrates the minor impact of the penetration depth on the airway closure

dynamics. The penetration depth is varied over three orders of magnitude, i.e. $\chi \in [0.001,\ 1]$, and the remaining parameters are set to the baseline values. Upon an increase of the penetration depth, fig. 6 shows a speed-up of the airway closure (about 5% faster for $\chi = 1$ than for $\chi = 0.001$) and sligthly increases the wall stress and stress gradients.

Similar observations can be extended to a variation of the adsorption and desorption coefficients, as well as to the Schmidt numbers. Decreasing $(\mathrm{K_a},\ \mathrm{K_d})$ and $(\mathrm{Sc},\ \mathrm{Sc_s})$ speeds up the airway closure, and has a negligible effect on the wall stresses. This is demonstrated in figs. 7 and 8, where $(\mathrm{K_a},\ \mathrm{K_d}) \in ([10^3,\ 10^5],\ [10,\ 10^3])$ and $(\mathrm{Sc},\ \mathrm{Sc_s}) \in ([1,\ 10],\ [10,\ 100])$, respectively. All the other parameters are set to the baseline values.

D. Effect of the Laplace number La

Another non-dimensional group varied in our study is the Laplace number. The rationale of performing a dedicated parametric study is two-fold: (i) we are interested in several bronchioles generations, whose Laplace number decays linearly with a, and (ii) we consider healthy and pathological cases, whose Laplace number can vary upon a change of σ_0. Three Laplace numbers are considered, i.e. La = 50, 100 and 500. Moreover, in order to mimic the difference between a healty patient and a surfactant deficient one, two values are assumed as reference for the initial surfactant concentration: (i) a clean case ($C_0 = 0$), and (ii) a surfactant contaminated case ($C_0 = 10^{-4}$). All the combinations between the the three Laplace numbers and the two initial concentrations are considered, for a total of six sets of parameters. All the other non-dimensional groups are set according to the baseline case.

Figure 9 shows the effect of a change of La for clean and contaminated cases. In order to ease the comprehension of our numerical results in the context of physiologically-relevant applications leading to an increase of surface tension, we plot the stresses and their axial gradient pre-multiplying them by La. This removes their dependence on σ_0 coming from the capillary scaling; moreover, for the same reason, we divide the dimensionless time t by La. This demonstrates that an increase of surface tension leads to the well expected acceleration of the Plateau–Rayleigh instability ($\sigma_0 \uparrow$ implies $\mathrm{La} \sim \sigma_0 \uparrow$ that leads to $\mu_\mathrm{L} a t_c/\sigma_0 \sim t_c/\mathrm{La} \downarrow$), as well as to an increase of the wall stress and stress gradient ($\sigma_0 \uparrow$ implies $\mathrm{La} \sim \sigma_0 \uparrow$ that leads, e.g. to $\sigma_0 \Delta p_\mathrm{w}/a \sim \mathrm{La} \Delta p_\mathrm{w} \uparrow$). We further stress that the increase of the stress level at epithelium due to surfactant deficiency can be as high as one order of magnitude (cf. data

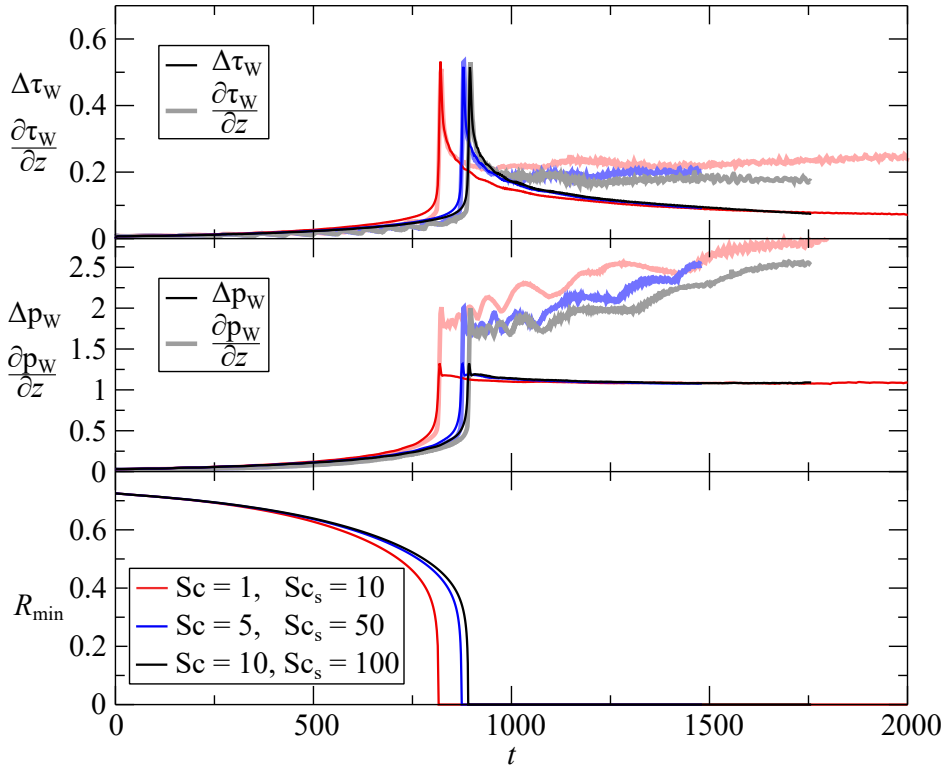

FIG. 8. Effect of the Schmidt numbers. Bottom: minimum of the radial location of the interface, R_I (solid line). Middle: excursion of the normal stress distribution along the wall, $\Delta p_{\rm w}(t) = \max_z p(r=1) - \min_z p(r=1)$ (light-colored bold line), and the maximum axial wall pressure gradient $\max|\partial_z p(r=1)|$ (dark-colored line). Top: excursion of the tangential stress distribution along the wall, $\Delta\tau_{\rm w}(t) = \max_z \tau(r=1) - \min_z \tau(r=1)$ (light-colored bold line), and the maximum axial wall shear stress gradient $\max|\partial_z \tau(r=1)|$ (dark-colored line). The bulk and interfacial Schmidt numbers, i.e. Sc and $\rm Sc_s$, respectively, are varied between $({\rm Sc},\ {\rm Sc_s}) \in ([1,\ 10],\ [10,\ 100])$, whereas the other simulation parameters are fixed: $C_0 = 10^{-4}$, La $= 100$, $\rm K_a = 10^4$, $\rm K_d = 10^2$, $\chi = 0.01$, $\beta = 0.7$, and $\varepsilon = 0.25$.

for La $= 50$ and La $= 500$ in the top and middle panels of fig. 9). These same conclusions are well in agreement with the data of [8].

The net effect of the surfactant concentration C_0 confirms the speeding up of the airway closure observed in fig. 4 upon an increase of surfactant concentration. Figure 9 generalizes the validity of such a result over the whole range of interest of the Laplace numbers for healthy and pathological human bronchioles. Once again, we stress that increasing the surfactant concentration has a minor impact on the stresses and their gradient at the airway

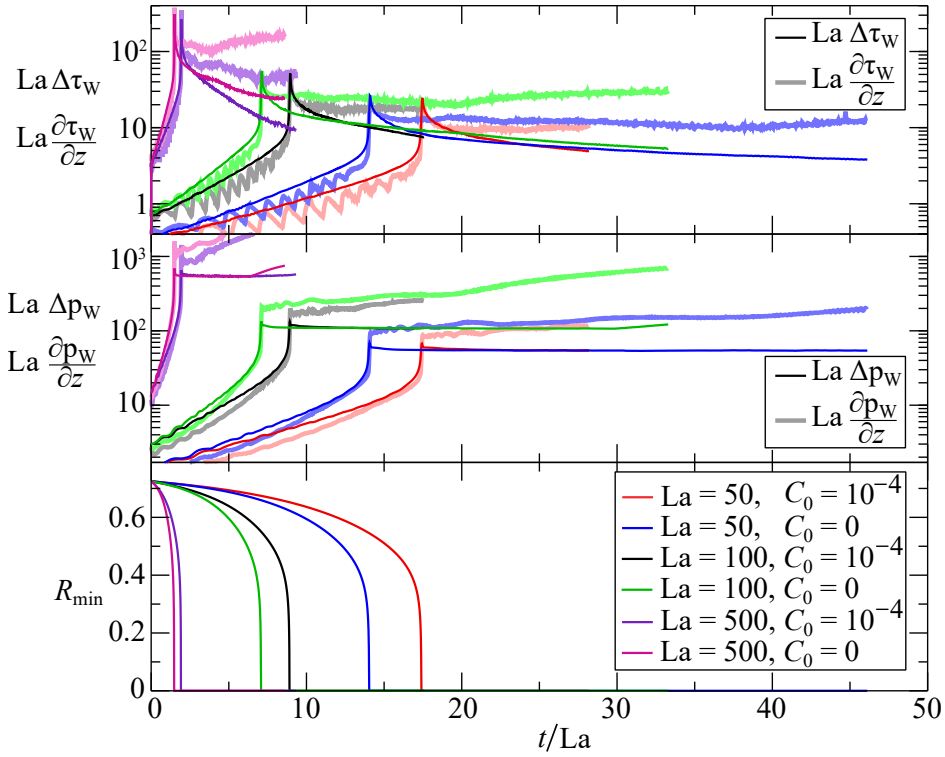

FIG. 9. Effect of the Laplace number. Bottom: minimum of the radial location of the interface, R_I (solid line). Middle: excursion of the normal stress distribution along the wall, $\Delta p_{\rm w}(t) = \max_z p(r=1) - \min_z p(r=1)$ (light-colored bold line), and the maximum axial wall pressure gradient $\max|\partial_z p(r=1)|$ (dark-colored line). Top: excursion of the tangential stress distribution along the wall, $\Delta\tau_{\rm w}(t) = \max_z \tau(r=1) - \min_z \tau(r=1)$ (light-colored bold line), and the maximum axial wall shear stress gradient $\max|\partial_z \tau(r=1)|$ (dark-colored line). The Laplace number and initial surfactant concentration, i.e. La and C_0, respectively, are varied between $({\rm La},\ C_0) \in ([50,\ 500],\ \{0,\ 10^{-4}\})$ for a total of six cases, whereas the other simulation parameters are fixed: ${\rm K_a} = 10^4$, ${\rm K_d} = 10^2$, $\chi = 0.01$, $\beta = 0.7$, ${\rm Sc} = 10$, ${\rm Sc_s} = 100$, and $\varepsilon = 0.25$.

wall (cf. clean and contaminated case in fig. 9).

E. Effect of the average non-dimensional film thickness ε

The last parametric study we carry out involves the average non-dimensional liquid film thickness ε. The physiological relevance of such a parameter is related to the pathologies inducing hypersecretion of mucus, hence enhancing ε.

Figure 10 depicts the effect of the average film thickness on the airway closure and it

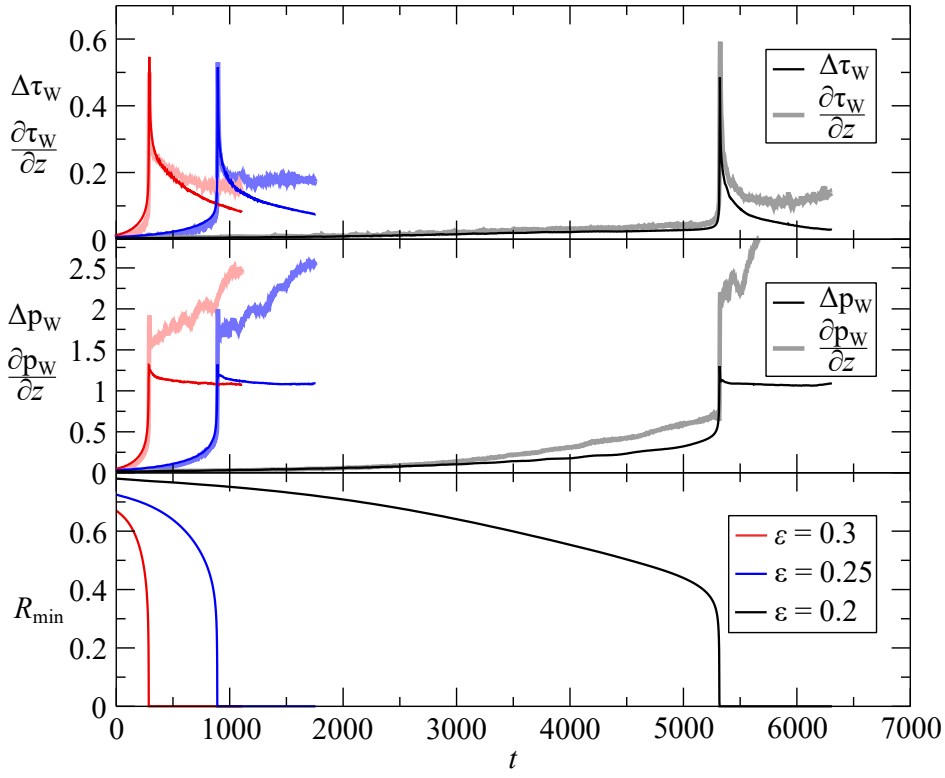

FIG. 10. Effect of initial liquid film thickness. Bottom: minimum of the radial location of the interface, R_I (solid line). Middle: excursion of the normal stress distribution along the wall, $\Delta p_{\rm w}(t) = \max_z p(r=1) - \min_z p(r=1)$ (light-colored bold line), and the maximum axial wall pressure gradient $\max|\partial_z p(r=1)|$ (dark-colored line). Top: excursion of the tangential stress distribution along the wall, $\Delta\tau_{\rm w}(t) = \max_z \tau(r=1) - \min_z \tau(r=1)$ (light-colored bold line), and the maximum axial wall shear stress gradient $\max|\partial_z \tau(r=1)|$ (dark-colored line). The average non-dimensional film thickness ε is varied between 0.2 and 0.3, whereas the other simulation parameters are fixed: $C_0 = 10^{-4}$, La = 100, Sc = 10, $\mathrm{Sc_s} = 100$, $\mathrm{K_a} = 10^4$, $\mathrm{K_d} = 10^2$, $\beta = 0.7$, and $\chi = 0.01$.

demonstrates that an increase of ε speeds up the Plateau–Rayleigh instability leading to airway closure on the wall stresses and tangential stress gradient. On the other hand, when considering the maximum normal stress gradient at the wall, $\max|\partial_z p_{\rm w}|$, a remarkable increase is observed, especially for the post-coalescence phase. This is due to the origin of the pressure gradient peak, produced by the capillary wave advected near the wall by the bifrontal plug growth (see [8]). In fact, in agreement with the asymptotic theory for a Bretherton bubble [53], the gradient of the pressure scales inversely proportional to the average film thickness, i.e. $\partial_z p_{\rm w} \approx -\varepsilon \partial_z^3 \tilde{h}$, where $\tilde{h} = 1 - R_{\rm I}$.

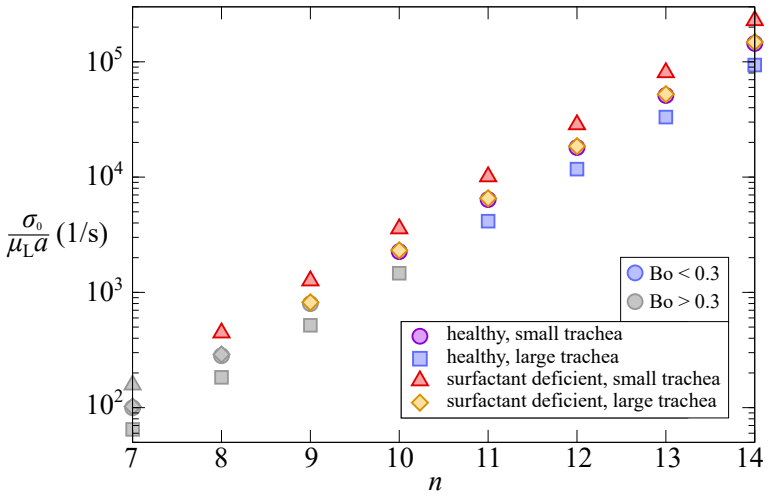

FIG. 11. Order-of-magnitude estimate of the inverse capillary time unit $T^{-1} = \sigma_0/\mu_L a$. The light-blue markers denote the working framework of our investigation for which gravitational effects are safely neglected (Bo < 0.3).

F. Stability diagram

Figure 11 reports an order-of-magnitude estimate of the inverse capillary time unit $T^{-1} = \sigma_0/\mu_L a$ for healthy and pathological cases of patients with large and small trachea. The gray markers denote the conditions for which gravitational effects cannot be neglected, hence our model does not strictly apply to them. Light-blue markers refer to the inverse airway capillary time unit of interest within our model framework. For pathological cases at the 8th and 9th generation the order of magnitude of T^{-1} is 500/s and 1000/s, respectively, whereas, including healthy cases for 10th and 11th generation, the order of magnitude of the inverse capillary time unit increases to 2000/s and 5000/s, respectively, for healthy individuals and to 3000/s and 8500/s for pathological patients. Considering that for healthy patients the respiratory rate is about 20/min (one breath every 3 seconds, [54]), the airway closure predicted in our model is considered physiologically relevant if it occurs before $t \approx 3 \times 2000 = 6000$ capillary time units at 10th generation, and $t \approx 3 \times 5000 = 15000$ capillary time units at 11th generation. The respiratory rate increases up to about 30/min for pathological conditions (one breath every 2 seconds, [54]), hence the critical time threshold for pathological cases reduces to $t \approx 2 \times 500 = 1000$ capillary time units at 8th generation, $t \approx 2 \times 1000 = 2000$ at 9th generation, while it increases to $t \approx 2 \times 3000 = 6000$ at 10th

generation, and $t \approx 2 \times 8500 = 17000$ capillary time units at 11th generation.

In the followings, the stability diagram of our airway closure model will be discussed on the light of the previous considerations about the time scales of the corresponding biological system. We will denote as *physiologically unstable* all the conditions leading to the formation of a liquid plug *within a breathing cycle*. Whenever the liquid plug does not form (unconditional stability) or when it forms too late (conditional stability), we will assume that the airway closure would not occur in a corresponding physiological system, and we denote such cases as *physiologically stable*.

The stability threshold of the airway closure is evaluated for La = 100, $\beta = 0.7$, Sc = 10, $\mathrm{Sc_s} = 100$, $\mathrm{K_a} = 10^4$, $\mathrm{K_d} = 10^2$, $\chi = 0.01$, $C_0 \in [0,\ 5 \times 10^{-4}]$, and $\varepsilon \in [0.125,\ 0.25]$. Figure 12 shows the minimum radial coordinate of the liquid-gas interface as a function of time for the 25 parameter sets resulting from the combination between the five average film thicknesses ε (color-coded from red to purple) and the five initial surfactant concentrations C_0 (one per panel row). The figure is presented in three columns in order to highlight three very different time scales of interest: (i) for the first column $t \in [0,\ 2000]$, (ii) for the second column $t \in [0,\ 5000]$, and (iii) for the third column $t \in [0,\ 30000]$. On the abscissae, the critical closure times (t_c) are indicated as a function of the physiological conditions (t_cp for pathological fast-breathing patients and t_ch for healthy patients with a regular breathing) and lung generation (e.g. t_cp8 denotes the critical closure time for the bronchioles of the 8th generation in a pathological patient). Such critical closure times correspond to the period of the breathing cycle (either 2 or 3 seconds for pathological $t_\mathrm{cp}T = 2$s and healthy conditions $t_\mathrm{ch}T = 3$s, respectively) non-dimensionalized with respect to the bronchioles radius at the corresponding generation and they represent the longest time an airway closure can take in our model to qualify as physiologically admissible (*physiologically unstable*).

A summary of the physiological stability conditions is reported in the three diagrams depicted in fig. 13 denoting with open markers the physiologically unstable configurations, while the full markers show the stable conditions. For fast-breathing pathological patients, the occlusion of distal airways can occur at generation 8 for a critical average thickness $\varepsilon_c \in [0.2,\ 0.225]$ if $C_0 \in [0,\ 10^{-4}]$ (see fig. 13(a)). In such case, an increase of the initial surfactant concentration up to $C_0 = 5 \times 10^{-4}$ induce an unconditionally stable condition that prevents airway closure from occurring for $\varepsilon \in [0.2,\ 0.225]$ (see black line in fig. 12) and shifts the critical condition to $\varepsilon_c \in [0.225,\ 0.25]$.

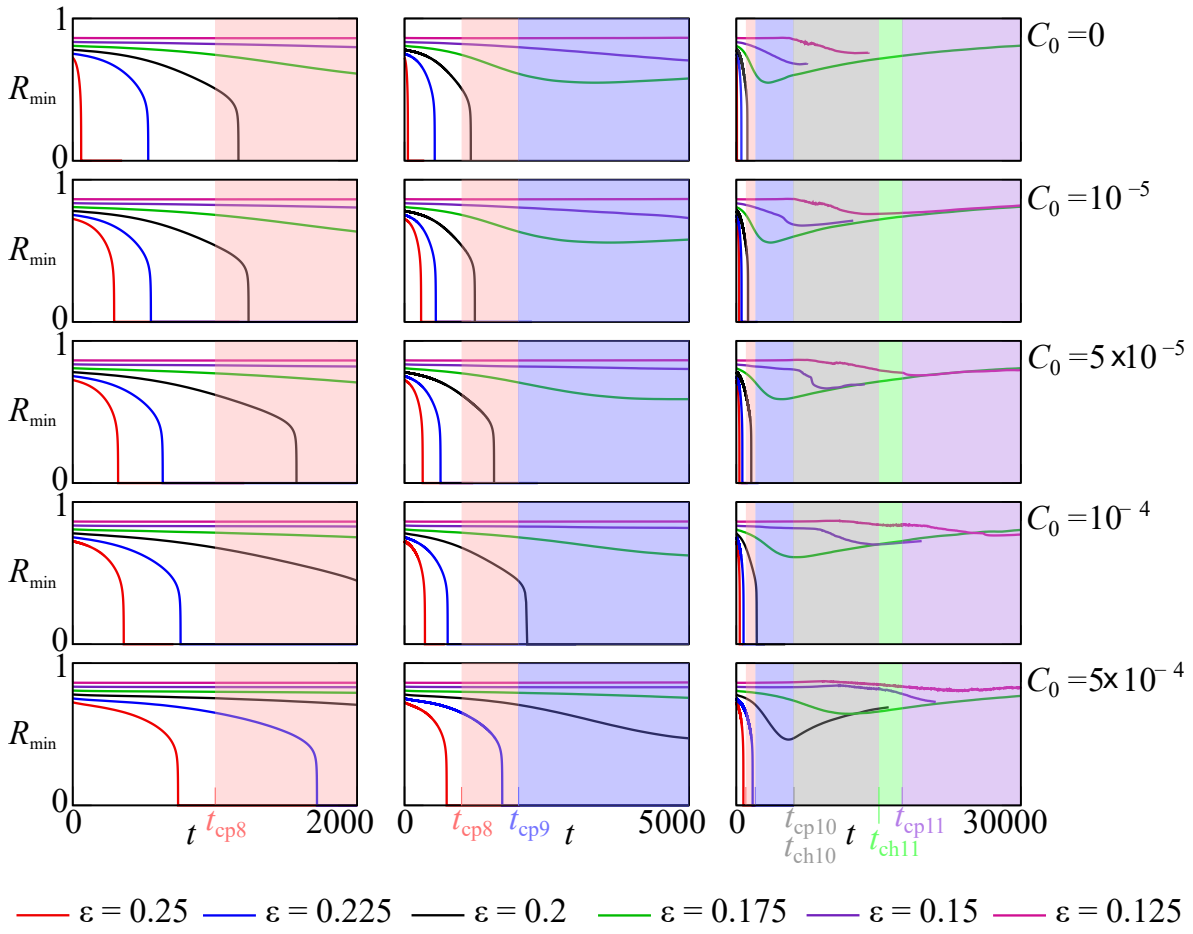

FIG. 12. Minimum of the radial location of the interface, R_I, color-coded for five average film thicknesses ($\varepsilon \in [0.125,\ 0.25]$) and arranged in rows each of which corresponds to one of the five initial surfactant concentrations $C_0 \in [0,\ 5 \times 10^{-4}]$. All the other parameters are fixed: La = 100, Sc = 10, $\mathrm{Sc_s}$ = 100, $\mathrm{K_a} = 10^4$, $\mathrm{K_d} = 10^2$, $\beta = 0.7$, and $\chi = 0.01$. Left, middle, and right panels denote the same airway closure dynamics over three relevant time scales: $t \in [0,\ 2000]$ (left), $t \in [0,\ 5000]$ (middle), and $t \in [0,\ 30000]$ (right). The critical closure times t_c are shown on the abscissae for pathological $t_{cp}T = 2$s and healthy conditions $t_{ch}T = 3$s, normalized on the characteristic capillary unit time of a given generation (e.g. t_{cp8} denotes the critical closure time at generation 8 for pathological fast-breathing patients).

When considering 9th-generation bronchioles of fast-breathing pathological patients (see fig. 13(b)), the physiologically critical average thickness reduces to $\varepsilon_c \in [0.175,\ 0.2]$ if $C_0 \in [0,\ 5 \times 10^{-5}]$ and $\varepsilon_c \in [0.2,\ 0.225]$ if $C_0 \in [10^{-5},\ 5 \times 10^{-5}]$. This decrease of stability

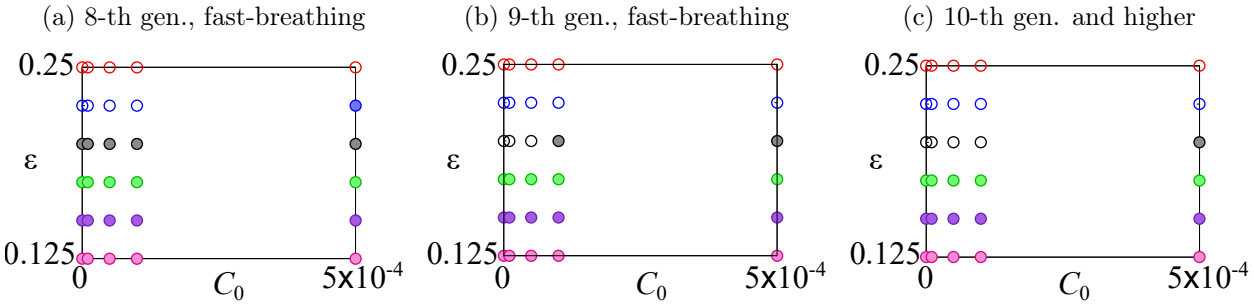

FIG. 13. Physiological stability diagram for bronchioles of: (a) 8th generation in fast-breathing pathological patients, (b) 9th generation in fast-breathing pathological patients, and (c) 10th and higher generations in all patients. Open markers denote physiologically unstable conditions, i.e. the airway closure occurs within a breathing cycle, while full markers depict physiologically stable cases.

of the system is well understood considering that the higher the generation, the smaller the bronchioles, and the more dominant the capillary forces become. Indeed, for distal airways the Plateau–Rayleigh instability at the origin of the airway closure leads more frequently to the occlusion of the airways when compared to lower-generation bronchioles. Such a stability loss is further confirmed by fig. 13(c) where 10th and higher generations are considered. The critical average film thickness reduces to $\varepsilon_c \in [0.175,\ 0.2]$ if $C_0 \in [0,\ 10^{-4}]$ and $\varepsilon_c \in [0.2,\ 0.225]$ if C_0 is 5×10^{-5}.

We further stress that such critical values are significantly higher than the value predicted by [3], i.e. $\varepsilon_c = 0.12$. The reason is that the critical thickness computed by [3] reflects the onset of the Plateau–Rayleigh instability for thin films, which instability is indeed observed in our simulations (see initial decrease of $R_{\min}$). However, the capillary instability gets further stabilized by the flow in the thick bulge and along the interface (see further increase of $R_{\min}$ after an initial decrease for $\varepsilon < 0.2$), which stabilization effect cannot be dealt with by employing lubrication theory.

V. SUMMARY AND CONCLUSIONS

The effect of surfactant in human airway closure has been investigated by proposing a model for liquid plug formation in distal airways. We decided to simplify our mathematical

model neglecting airway wall deformability, mobile ciliated surfaces and non-Newtonian effects. As a result, we focus on: (i) the coupling between the bulk and interfacial surfactant dynamics (neglecting the surfactant micelles), (ii) the Plateau–Rayleigh instability at the core of the airway closure, and (iii) the bifrontal plug growth leading to a sudden post-coalescence increase of the stress level.

An extensive parametric study has been carried out by setting a baseline of reference for all the flow and surfactant parameters, and varying (almost always) one parameter at a time. The aim is to evaluate the standalone effect of each parameter.

At first, we varied the initial surfactant concentration showing that an increase of C_0 can well have a remarkable impact on the Plateau–Rayleigh instability, postponing it significantly when increasing it from the clean case ($C_0 = 0$) to the most contaminated case we consider ($C_0 = 5 \times 10^{-4}$). Moreover, we observed a corresponding decrease of 20% of the tangential stress and stress gradient at the wall. Both such effects are also achieved by increasing the strength of the surfactant signified by the elasticity number β and they are both beneficial effects for the mechanics of a physiological airway closure. Therefore, our results show that the biological production of surfactant in human lungs does not have any negative *mechanical* effect as they help to prevent airway closure and, when it occurs, they limit the stress level on the epithelium.

The other non-dimensional numbers characterizing the surfactant have little impact on the airway closure. In fact, varying over several orders of magnitude Sc, $\mathrm{Sc_s}$, $\mathrm{K_a}$, $\mathrm{K_d}$, and χ, only minor effects on the main dynamics of the pre- and post-coalescence phases are observed. This highlights the general application of our results, as they are not very sensitive to the model parameters mimicking the surfactant dynamics in the bulk and at the interface. Moreover, our considerations also point towards good design rules for enhancing the performance of surfactant replacement therapies. In fact, rather than focusing on producing surfactant that dissolve faster/slower, penetrate deeper/shallower and adsorbe/desorbe more or less efficiently, from the sole mechanical point of view, a beneficial surfactant replacement therapy should aim for high β and large enough C_0. As also observed by other surfactant replacement mathematical models [55], too high surfactant concentrations are expected to saturate the benefit of corresponding surfactant replacement protocols.

Another parameter varied in our study is the Laplace number La. Upon an increase of the surface tension, the airway closure gets speed up with a consequent increase of the wall

stress and stress gradient. It is remarkable that a surfactant deficiency brings the Laplace number from La = 50 to La = 500, leading to a one-order-of-magnitude increase of the stress level at epithelium.

The last parameter we investigated is the average liquid film thickness ε. We show that airway closure with a thin liquid film is more dangerous because the pressure gradient produced by the corresponding post-coalescence capillary wave is larger. However, low ε significantly delays the closure, hence tending to physiologically stabilize the process (in agreement with the experiments carried out by [19]). In this sense, airway closure with a thick film is expected to be much more frequent and probable than for thin liquid layers.

Finally, a dedicated two-parameter stability analysis in terms of ε and C_0 has been carried out to investigate the effect of surfactant concentration for various liquid film thicknesses. Our results are produced for an initial perturbation of $A = 10\%$, and considering initial perturbations smaller than ours would lead to longer closure times. This calls for an adjustment of the physiological stability diagram in order to generalize our findings. Such a correction can be done by considering that the lubrication theory predicts a growth of the interfacial perturbation amplitude as $A = A_0 e^{gt+ikz}$, where A_0 is the initial amplitude, k the wavenumber, and $g = k^2(1-k^2)/3$ [56]. The exponential growth predicted by the lubrication theory holds for infinitesimal amplitudes up to amplitudes larger than our $A = 10\%$ [57]. Hence, $A = A_0 e^{gt+ikz}$ can be used to calculate the time required by an arbitrary perturbation smaller than ours to lead to $A = 10\%$. The corresponding amplitude-growing time shall be added to our t_c for adjusting the physiological stability diagram whether an arbitrary perturbation smaller than 10% is considered. The conclusion of our physiological stability study points out that the increase of surfactant concentration shifts towards higher lung generations the occurrence of airway closure, in agreement with [10].

ACKNOWLEDGMENTS

Support from National Institutes of Health (NIH), grant number R01-HL136141, and the Scientific and Technical Research Council of Turkey, (TUBITAK), grant number 119M513, is kindly acknowledged.

[1] JH Widdicombe, SJ Bastacky, DX Wu, and CY Lee, "Regulation of depth and composition of airway surface liquid," European Respiratory Journal **10**, 2892–2897 (1997)

[2] C. S. Kim M. A. Sackner, "Phasic flow mechanisms of mucus clearance," Eur. J. Respir. Dis. Suppl. **153**, 159–164 (1987)

[3] P. A. Gauglitz and C. J. Radke, "An extended evolution equation for liquid film breakup in cylindrical capillaries," Chem. Eng. Sci. **43**, 1457–1465 (1988)

[4] P. T. Macklem, D. F. Proctor, and J. C. Hogg, "The stability of peripheral airways," Resp. Physiol. **8**, 191–203 (1970)

[5] I. A. Greaves, J. Hildebrandt, and J. F.G. Hoppin, *Micromechanics of the lung*, Vol. 3 (American Physiological Society, 1986)

[6] Joseph Antoine Ferdinand Plateau, *Statique expérimentale et théorique des liquides soumis aux seules forces moléculaires*, Vol. 2 (Gauthier-Villars, 1873)

[7] Lord Rayleigh, "On the instability of cylindrical fluid surfaces," Phil. Mag. **34**, 177–180 (1892)

[8] F Romanò, H Fujioka, M Muradoglu, and j B Grotberg, "Liquid plug formation in an airway closure model," Physical Review Fluids **4**, 093103(1–23) (2019)

[9] D. Halpern and J. B. Grotberg, "Fluid-elastic instabilities of liquid-lined flexible tubes," J. Fluid Mech. **244**, 615–632 (1992)

[10] D. Halpern and J. B. Grotberg, "Surfactant effects on fluid-elastic instabilities of liquid-lined flexible tubes: a model of airway closure," J. Biomech. Eng. **115**, 271–277 (1993)

[11] D. Halpern, H. Fujioka, and J. B. Grotberg, "The effect of viscoelasticity on the stability of a pulmonary airway liquid layer," Phys. Fluids **22**, 011901 (2010)

[12] O Erken, F Romanò, JB Grotberg, and M Muradoglu, "Capillary instability of a two-layer annular film: an airway closure model," Journal of Fluid Mechanics **934** (2022)

[13] M. Heil, A. L. Hazel, and J. A. Smith, "The mechanics of airway closure," Resp. Physiol. Neurobi. **163**, 214–221 (2008)

[14] C. F. Tai, S. Bian, D. Halpern, Y. Zheng, M. Filoche, and J. B. Grotberg, "Numerical study of flow fields in an airway closure model," J. Fluid Mech. **677**, 483–502 (2011)

[15] D. Huh, H. Fujioka, Y. C. Tung, N. Futai, R. Paine, J. B. Grotberg, and S. Takayama, "Acoustically detectable cellular-level lung injury induced by fluid mechanical stresses in microfluidic

airway systems," P. Nat. Acad. Sci. USA **104**, 18886–18891 (2007)

[16] A. M. Bilek, K. C. Dee, and D. P. Gaver, "Mechanisms of surface-tension-induced epithelial cell damage in a model of pulmonary airway reopening," J. Appl. Physiol. **94**, 770–783 (2003)

[17] S. S. Kay, A. M. Bilek, K. C. Dee, and D. P. Gaver, "Pressure gradient, not exposure duration, determines the extent of epithelial cell damage in a model of pulmonary airway reopening," J. Appl. Physiol. **97**, 269–276 (2004)

[18] S. Bian, C. F. Tai, D. Halpern, Y. Zheng, and J. B. Grotberg, "Experimental study of flow fields in an airway closure model," J. Fluid Mech. **647**, 391–402 (2010)

[19] KJ Cassidy, D Halpern, BG Ressler, and JB Grotberg, "Surfactant effects in model airway closure experiments," Journal of Applied Physiology **87**, 415–427 (1999)

[20] F Romanò, H Fujioka, M Muradoglu, and j B Grotberg, "The effect of viscoelasticity in an airway closure model," Journal of Fluid Mechanics **913** (2021)

[21] M Muradoglu, F Romanò, H Fujioka, and J B Grotberg, "Effects of surfactant on propagation and rupture of a liquid plug in a tube," Journal of Fluid Mechanics **872**, 407–437 (2019)

[22] S. N. Ghadiali and D. P. Gaver, "Biomechanics of liquid-epithelium interactions in pulmonary airways," Resp. Physiol. Neurobi. **163**, 232–243 (2008)

[23] Y Hu, F Romanò, and JB Grotberg, "Effects of surface tension and yield stress on mucus plug rupture: a numerical study," J. Biomech. Eng. **142**, 061007 (2020)

[24] S Amir Bahrani, Souria Hamidouche, Masoud Moazzen, Khady Seck, Caroline Duc, Metin Muradoglu, James B Grotberg, and Francesco Romanò, "Propagation and rupture of elastoviscoplastic liquid plugs in airway reopening model," Journal of Non-Newtonian Fluid Mechanics , 104718 (2021)

[25] Y. Zheng, H. Fujioka, S. Bian, Y. Torisawa, D. Huh, S. Takayama, and J. B. Grotberg, "Liquid plug propagation in flexible microchannels: A small airway model," Phys. Fluids **21**, 071903 (2009)

[26] J. B. Grotberg, "Pulmonary flow and transport phenomena," Ann. Rev. Fluid Mech. **26**, 529–571 (1994)

[27] James B Grotberg, "Respiratory fluid mechanics and transport processes," Annual review of biomedical engineering **3**, 421–457 (2001)

[28] James B Grotberg and Oliver E Jensen, "Biofluid mechanics in flexible tubes," Annu. Rev. Fluid Mech. **36**, 121–147 (2004)

[29] James B Grotberg, *Biofluid Mechanics: Analysis and Applications* (Cambridge University Press, 2021)

[30] G. Tryggvason, R. Scardovelli, and S. Zaleski, *Direct Numerical Simulations of Gas-Liquid Multiphase Flows* (Cambridge University Press, 2011)

[31] H. Fujioka and J. B. Grotberg, "The steady propagation of a surfactant-laden liquid plug in a two dimensional channel," Phys. Fluids **17**, 082102 (2005)

[32] Y. Zheng, H. Fujioka, and J. B. Grotberg, "Effects of gravity, inertia, and surfactant on steady plug propagation in a two-dimensional channel," Phys. Fluids **19**, 082107 (2007)

[33] H. Fujioka, D. Halpern, and D. P. Gaver III, "A model of surfactant-induced surface tension effects on the parenchymal tethering of pulmonary airways," Journal of Biomechanics **46**, 319–328 (2013)

[34] H. A. Stone, "A simple derivation of the time-dependent convective-diffusion equation for surfactant transport along a deforming interface," Phys. Fluids **A2**, 111–112 (1990)

[35] M. Muradoglu and G. Tryggvason, "A front-tracking method for computation of interfacial flows with soluble surfactants," J. Comput. Phys. **227**, 2238–2262 (2008)

[36] M. Muradoglu and G. Tryggvason, "Simulations of soluble surfactants in 3d multiphase flow," J. Comput. Phys. **274**, 737–757 (2014)

[37] F. H. Harlow and J. E. Welch, "Numerical calculation of time-dependent viscous incompressible flow of fluid with free surface," Phys. Fluids. **8**, 2182–2189 (1965)

[38] S. O. Unverdi and G. Tryggvason, "A front-tracking method for viscous incompressible multi-phase flows," J. Comput. Phys. **100**, 25–37 (1992)

[39] R. Borges, M. Carmona, B. Costa, and W. Don, "An improved weighted essentially non-oscillatory scheme for hyperbolic conservation laws," J. Comput. Phys. **110**, 859–864 (2013)

[40] U. Olgac, A. D. Kayaalp, and M. Muradoglu, "Buoyancy-driven motion and breakup of viscous drops in constricted capillaries," Int. J. Multiphase Flows **32**, 1055–1071 (2006)

[41] G. Tryggvason, B. Bunner, A. Esmaeeli, D. Juric, N. Al-Rawahi, W. Tauber, J. Han, S. Nas, and Y.-J. Jan, "A front-tracking method for the computations of multiphase flow," J. Comput. Phys. **169**, 708–759 (2001)

[42] C. Peskin, "Numerical analysis of blood flow in the heart," J. Comput. Phys. **25**, 220–252 (1977)

[43] Ewald R Weibel, André Frédérick Cournand, and Dickinson W Richards, *Morphometry of the human lung*, Vol. 1 (Springer, 1963)

[44] R. G. Crystal, *The Lung: Scientific Fundations* (Lippincott, 1997)

[45] J. A. Clements, E. S. Brown, and R. P. Johnson, "Pulmonary surface tension and the mucus lining of the lungs: some theoretical considerations," Journal of Applied Physiology **12**, 262–268 (1958)

[46] J. H. Widdicombe, "Regulation of the depth and composition of airway surface liquid," Journal of Anatomy **201**, 313–318 (2002)

[47] JR Lister, JM Rallison, AA King, LJ Cummings, and OE Jensen, "Capillary drainage of an annular film: the dynamics of collars and lobes," Journal of Fluid Mechanics **552**, 311–343 (2006)

[48] D. R. Otis, E. P. Ingenito, R. D. Kamm, and M. Johnson, "Dynamic surface tension of surfactant TA: experiments and theory," J. Appl. Physiol. **77**, 2681–2688 (1994)

[49] M. A. Launois-Surpas, T. IvanovaI, I. Panaiotov, J. E. Proust, F. Puisieux, and G. Georgiev, "Behavior of pure and mixed dppc liposomes spread or adsorbed at the air-water-interface," Colloid Polym. Sci. **270**, 901–911 (1992)

[50] M. L. Agrawal and R. D. Neuman, "Surface diffusion in monomolecular films, II. experiment and theory," J. Colloid. Interface Sci. **121**, 366–379 (1988)

[51] S. Schurch, H. Bachofen, J. Goerke, and F. Possmayer, "A captive bubble method reproduces the in situ behavior of lung surfactant monolayers," J. Appl. Physiol. **67**, 2389–2396 (1989)

[52] V.G. Levich, *Physicochemical Hydrodynamics* (Prentice Hall, Englewood Cliffs, NJ, USA, 1962)

[53] F. P. Bretherton, "The motion of long bubbles in tubes," J. Fluid Mech. **10**, 166–188 (1961)

[54] Michelle A Cretikos, Rinaldo Bellomo, Ken Hillman, Jack Chen, Simon Finfer, and Arthas Flabouris, "Respiratory rate: the neglected vital sign," Medical Journal of Australia **188**, 657–659 (2008)

[55] Marcel Filoche, Cheng-Feng Tai, and James B Grotberg, "Three-dimensional model of surfactant replacement therapy," Proceedings of the National Academy of Sciences **112**, 9287–9292 (2015)

[56] P. S Hammond, "Nonlinear adjustment of a thin annular film of viscous fluid surrounding a thread of another within a circular pipe," Journal of Fluid Mechanics **137**, 363–384 (1983)

[57] D. Halpern and J. B. Grotberg, "Nonlinear saturation of the rayleigh instability due to oscillatory flow in a liquid-lined tube," Journal of Fluid Mechanics **492**, 251–270 (2003)